THE RESPONSE OF FISSION GAS BUBBLES TO THE DYNAMIC BEHAVIOR OF POINT DEFECTS

J.M. GRIESMEYER and N.M. GHONIEM

School of Engineering and Applied Science, University of California, Los Angeles, USA

A model has been developed to investigate the response of fission gas bubbles to the dynamic behavior of uranium point defects in uranium oxide. Simple thermodynamics is used to calculate the thermal equilibrium concentrations of both anion and cation point defects in $UO_{2\pm x}$ and fully dynamic rate theory has been extended to estimate the dynamic concentrations of uranium vacancies and interstitials and the enhanced self-diffusion of uranium during constant temperature and thermal transient irradiations.

During low temperature irradiations, fission production of uranium Frenkel pairs is dominant and the slow migration rate of the vacancies leads to long start-up transients ($\sim 10^6$ s in stoichiometric UO_2 at 1000 K) as the vacancies reach a quasi-steady state with the microstructure. Thermal ramp behavior of the point defects and fission gas cavities depends primarily upon the initial concentration of point defects, and the temperature at which the thermal production of point defects becomes dominant. Our results indicate that non-equilibrium fission gas behavior is important for both constant temperature and thermal transient irradiations and that fission gas bubble behavior models must consider fuel stoichiometry. Below about 2200 K the dynamic behavior of the point defects should be incorporated as well.

1. Introduction

Safe operation of fast reactors necessitates the understanding of fuel behavior during reactivity excursions associated with accidents and abnormal operation. Fission gas bubbles are now recognized to be the major cause of swelling in uranium oxide fuels. Their swelling behavior determines the level of stresses imposed on the fuel element, and consequently the mode of failure. During the course of an accident, fuel temperature can increase rapidly from normal operating temperatures to near the melting point in a few seconds [1].

Previous theoretical models [2–5], used to predict fuel swelling due to fission gases, have utilized the argument that at high temperatures fission induced cavities behave like equilibrium gas bubbles. This means that under all conditions, the bubble radius is determined by a balance between the internal gas pressure and the surface tension force. However, a number of investigators have considered the cavity behavior under non-equilibrium circumstances where the irradiation field [6], temperature variations [7] or stress [8] alter this situation.

The objective of this work is to focus on the role of point defects on the growth of bubbles during steady state and transient operation. The results of the present investigation will serve as an input to a more comprehensive fission gas bubble behavior model [9]. In this model, the accurate determination of bubble radial changes under different irradiation conditions is of crucial importance.

Off-stoichiometric uranium oxide fuels contain point defects far in excess of the thermodynamic equilibrium values. When irradiation produced point defects are also considered, the situation is further complicated. On the other hand, a temperature transient influences both the number densities and migration behavior of these defects. Qualitatively, one would expect considerable variations of the time scales during which bubble gas atoms, vacancies and interstitials respond to rapid heating. The model presented here, which is based on homogeneous chemical kinetics rate theory, is aimed at quantifying these aspects. It is also developed to investigate the effects of important variables, such as stoichiometry, fuel heating rate, point defect fission yield, and microstructure on the final response of fission induced cavities.

While the details of the model and some of its prominent computational aspects are given in sections 2 and 3, it is important to state the assumptions employed throughout the calculations:

i. The fuel is preirradiated such that the nucleation stage of gas cavities has been surpassed. Here, we only study the growth aspects of these cavities.

ii. The number density of gas cavities, grain size and dislocation density do not change during irradiation.

iii. Fuel structure near the gas cavity surface is no different from the bulk (i.e. $UO_{2\pm x}$). Therefore, the response of gas cavities is mainly controlled by the slowly moving species (metal defects).

iv. We will not consider the effects of fission fragment collision cascade collapse on point defect populations. Hence, a homogeneous dynamic rate theory is used.

v. Bubble coalescence and re-solution effects are not treated in this work, but they are considered in the comprehensive model [9].

2. Equilibrium point defect concentrations

Materials with a fluorite structure, such as $UO_{2\pm x}$, contain more than one type of point defect. In contrast to metals, where only metal vacancies and interstitials exist, both anion and cation point defects play an important role. In this section, we will briefly discuss the method used to calculate anion as well as cation point defect concentrations. The following definitions characterize the quantities used in our analysis:

Quantities:
N = concentration, cm^{-3},
C = fractional concentration, number per site,
Subscripts:
s = lattice sites for ions or interstitials,
u = uranium ions,
o = oxygen ions,
v = vacancies,
i = interstitials,
S = Schottky type defect,
F = Frenkel type defect.
Superscripts:
4^+, q^+ = designates charge on ions considered,

Example:
$C_{vo} \equiv N_{vo}/N_{so} \equiv$ oxygen vacancy fractional concentration.

With this unified notation, the following relationships can be easily derived:

$$N_{su} = N_u^{4+} + N_u^{q+} + N_{vu} ,\qquad(1)$$

$$N_{so} = N_o + N_{vo} ,\qquad(2)$$

$$N_{so} = 2N_{su} ,\qquad(3)$$

$$N_{si} = N_{su} .\qquad(4)$$

Eqs. (1) and (2) express the conservation of cation and anion sites, respectively, while eqs. (3) and (4) reflect the UO_2 fluorite structure. To determine the point defect concentrations as well as the number of u atoms in the +3 or +5 state, the solution of five independent equations is required, as is described below.

The equilibrium concentration of Schottky defects is given by

$$C_{vu}C_{vo}^2 = e^{-\Delta G_S/kT} \equiv K_S ,\qquad(5)$$

where ΔG_S is the energy of formation of a Schottky defect, k is the Boltzmann constant, T is the irradiation temperature and K_S is the Schottky constant. On the other hand, the concentration of Frenkel defects can be written as

$$C_{vo}C_{io} = e^{-\Delta G_{Fo}/kT} \equiv K_{Fo}\qquad(6)$$

and

$$C_{vu}C_{iu} = e^{-\Delta G_{Fu}/kT} \equiv K_{Fu} ,\qquad(7)$$

where K_{Fo} and K_{Fu} are the Frenkel constants for oxygen and uranium, respectively. Additional relationships for conditions of electrical neutrality and ratio of oxygen to metal are:

$$4N_u^{4+} + qN_u^{q+} + 4N_{iu} = 2N_o + 2N_{oi} ,\qquad(8)$$

and

$$\frac{O}{U} = \frac{N_o + N_{oi}}{N_u^{q+} + N_u^{4+} + N_{iu}} = 2 + x .\qquad(9)$$

A fairly straightforward manipulation of eqs. (5)–(9)

Table 1
Point defect formation and migration energies in eV

ΔG_{Fo}	3.1 [10]
ΔG_{Fu}	9.5 [10]
ΔG_S	6.4 [10]
E_{vo}^m	0.25 [11], 1.7 [10]
E_{io}^m	1.0 [10]
E_{vu}^m	2.4 [10]
E_{iu}^m	1.9 [10]

results in a quartic equation in the variable C_{vo}:

$$\frac{K_{Fu}}{K_S}[C_{vo}]^4 + [C_{vo}]^3 \pm \tfrac{1}{2}x[C_{vo}]^2 - \tfrac{1}{2}K_{Fo}[C_{vo}] - K_S = 0.$$

(10)

The $+\tfrac{1}{2}x$ corresponds to hyperstoichiometric, while the $-\tfrac{1}{2}x$ corresponds to hypostoichiometric fuel compositions. Fractional concentrations of the other point

defects can immediately be calculated from eqs. (5)–(7).

Using the values of the parameters of table 1, and solving equations (5)–(7) and (10) will yield the fractional concentrations at any desired temperature and stoichiometry. For example, figs. 1–3 show the equilibrium fractional point defect concentrations as a function of temperature for hyperstoichiometric, hypostoichiometric and stoichiometric fuels. When the oxygen to metal ratio deviates considerably from the stoichiometric value ($x > 0.05$), various simplifications of eq. (10) can be used [16].

It is shown on figs. 1 and 3 that the uranium vacancy concentration is much larger than its interstitial counterpart for both stoichiometric and hyperstoichiometric oxides, over the whole temperature range. On the other hand, fig. 2 shows that the uranium interstitial concentration is larger than the vacancy concentration at low temperatures. The effective interstitial formation energy is about half
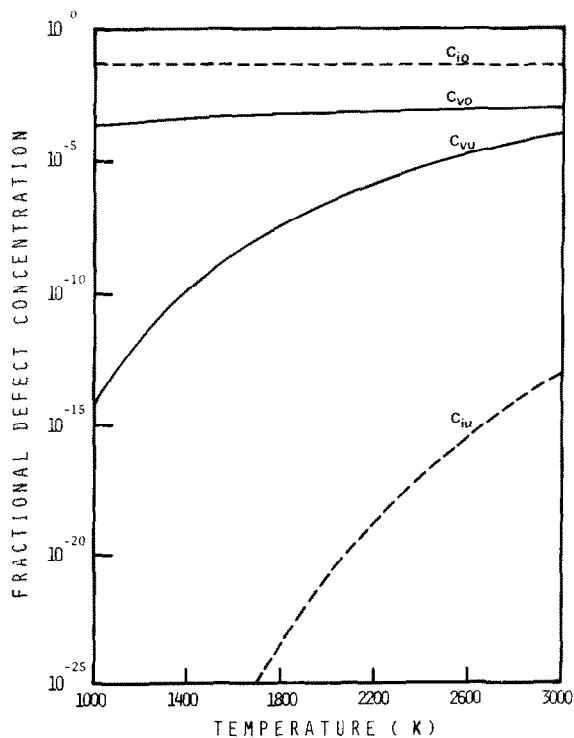

Fig. 1. Thermal defect concentrations as a function of temperature for O/M = 2.05.
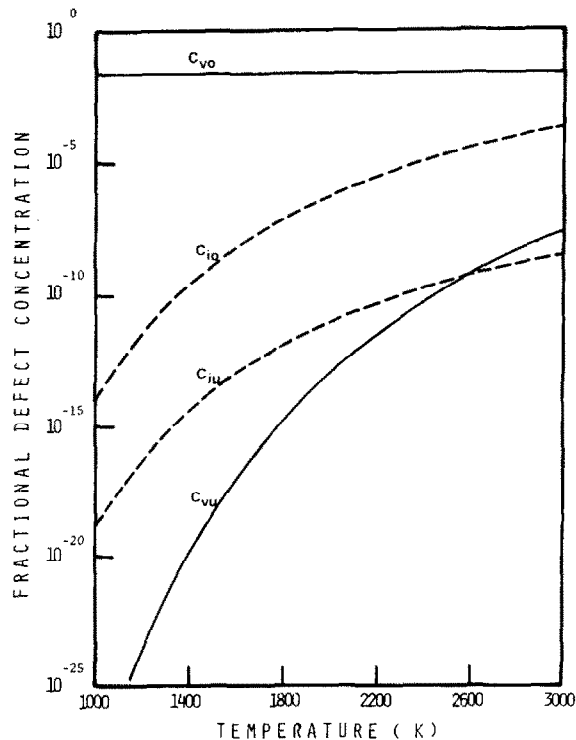

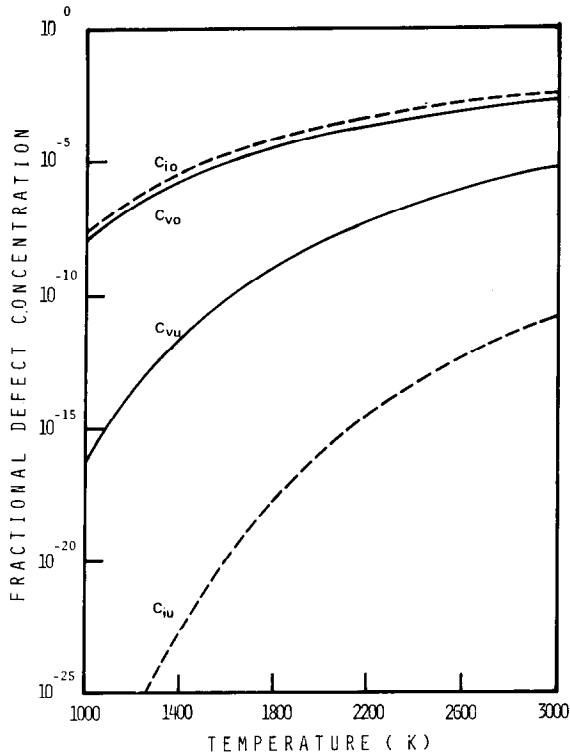Fig. 2. Thermal defect concentrations as a function of temperature for O/M = 1.95.

Fig. 3. Thermal defect concentrations as a function of temperature for O/M = 2.00.

the corresponding value for vacancies, which renders the interstitial concentration a larger value at low temperatures. However, at high temperatures the interstitial exponential term saturates, while the larger pre-exponential allows the vacancy concentration to become greater than the interstitial concentration.

Calculations of the thermodynamic equilibrium concentrations of the various kinds of point defects, provided in this section, determine the matrix point defect thermal population levels which define flow and emission rates, as described in the next section.

3. Analytical model

The rate theory framework provides a convenient method for studying the space averaged behavior of point defects and their subsequent effects on fission gas bubble growth. The fully dynamic rate theory (FDRT) [12] has been developed to analyze the

response of metals to pulsed and transient modes of irradiation, and is extended here to study $UO_{2 \pm x}$ fuel behavior in transients.

Rates of point defect production as well as their removal by different processes constitute the fundamental rate equations. In a mathematical formulation that incorporates the kinetic behavior of different irradiation produced species, there exists a wide variety of time constants. A time constant, λ as defined here, is the inverse of the time required to go through one e-folding change in a particular property.

3.1. Removal rates

Since the time constants of single point defects depend on the microstructure present at a particular instant, they are explicit functions of the metal's microstructure, and therefore, implicit functions of time. Their microstructural dependence can be simply expressed as [12]:

$$\lambda_i = \lambda_i^d + \lambda_i^C + \lambda_i^{GB}, \tag{11}$$

$$\lambda_v = \lambda_v^d + \lambda_v^C + \lambda_v^{GB}, \tag{12}$$

$$\lambda_i^d = \rho_d D_i Z_i, \tag{13}$$

$$\lambda_i^C = 4\pi N_C R_C D_i, \tag{14}$$

$$\lambda_i^{GB} = 6\sqrt{D_i(\lambda_i^d + \lambda_i^C)}/d, \tag{15}$$

$$\lambda_v^d = \rho_d D_v Z_v, \tag{16}$$

$$\lambda_v^C = 4\pi N_C R_C D_v, \tag{17}$$

$$\lambda_v^{GB} = 6\sqrt{D_v(\lambda_v^d + \lambda_v^C)}/d, \tag{18}$$

where λ_i is the total interstitial time constant, s^{-1}, λ_v is the total vacancy time constant, s^{-1}, λ_i^d is the interstitial time constant due to dislocations, s^{-1}, λ_i^C is the interstitial time constant due to cavities, s^{-1}, λ_i^{GB} is the interstitial time constant due to grain boundaries, s^{-1}, λ_v^d is the vacancy time constant due to dislocations, s^{-1}, λ_v^C is the vacancy time constant due to cavities, s^{-1}, λ_v^{GB} is the vacancy time constant due to grain boundaries, s^{-1}, ρ_d is the total dislocation density, cm^{-2}, D_i is the interstitial diffusion coefficient, cm^2/s, D_v is the vacancy diffusion coefficient, cm^2/s,

Z_i is the interstitial dislocation bias factor ($Z_i = 1.02$ in these calculations), Z_v is the vacancy dislocation bias factor ($Z_v = 1.00$ in these calculations), N_C is the concentration of cavities (bubbles), cm^{-3}, R_C is the cavity (bubble) radius, cm, d is the grain diameter, cm.

The relative importance of a particular sink with regard to the dynamic behavior of point defects is manifested in its specific removal rate. Individual sink removal rates are first order reactions which can be expressed as their relevant time constant, λ, multiplied by the temporal concentration of point defects. However, mutual recombination of point defects is a second order reaction that depends on the product of both concentrations. Different point defect removal rates are expressed as:

$$P_{si} = \lambda_i C_i , \qquad (19)$$

$$P_{sv} = \lambda_v C_v , \qquad (20)$$

$$P_r = \alpha C_v C_i , \qquad (21)$$

$$\alpha = g(D_i + D_v) , \qquad (22)$$

where P_{si} is the total sink removal rate for interstitials, s^{-1}, P_{sv} is the total sink removal rate for vacancies, s^{-1}, P_r is the total recombination rate of vacancies and interstitials, s^{-1}, α is the recombination coefficient, s^{-1}, g is a constant, cm^{-2}, C_v is the total fractional vacancy concentration, at/at, C_i is the total fractional interstitial concentration, at/at.

3.2. Emission rates

At high temperatures, the probability of emitting point defects from a cavity becomes appreciable. A larger cavity surface tension enhances vacancy emission, while it reduces interstitial emission from the surface. On the other hand, the pressure due to gas atoms inside the cavity has the opposite effect. A mathematical description of the emission process is given by [12]:

$$P_C^{ve} = \lambda_i^C C_{vu} \exp \{F_m \Omega/kT\} , \qquad (23)$$

$$P_C^{ie} = \lambda_i^C C_{iu} \exp \{-F_m \Omega/kT\}, \qquad (24)$$

where P_C^{ve} is the vacancy emission rate from cavity surface, s^{-1}, P_C^{ie} is the interstitial emission rate from cavity surface, s^{-1}.

The equilibrium concentrations of metal point defects C_{vu} and C_{iu} are determined from eqs. (5)–(7) and (10). It is important to note that for hypostoichiometric uranium oxide fuels, metal thermal interstitial concentration is appreciable, and interstitial diffusion becomes the dominant mechanism for atom transport [10].

The mechanical force per unit surface area of the cavity, F_m, can be expressed as

$$F_m = p + 2\gamma/R_C - p_g . \qquad (25)$$

Here p is the hydrostatic pressure, γ the surface energy, and p_g the gas pressure. F_m is the pressure misbalance at the cavity surface. In determining the gas pressure p_g, the modified Van der Waals law was used.

Deformation produced dislocations act also as thermal sources for point defects. For simplicity of calculations, all dislocations are assumed to be of the edge type. Emission rates of uranium vacancies and interstitials can now be expressed as

$$P_d^{ve} = \lambda_v^d C_{vu} , \qquad (26)$$

$$P_d^{ie} = \lambda_i^d C_{iu} , \qquad (27)$$

where P_d^{ve} and P_d^{ie} are the emission rates in at/at · s of uranium vacancies and interstitials, respectively. Emission rates of vacancies and interstitials from grain boundaries are given by similar expressions.

Total emission rates are simply the sums of individual rates. Therefore, for vacancies, the total emission rate is

$$P_{tot}^{ve} = P_C^{ve} + P_d^{ve} + P_{GB}^{ve} + P_R^{iv} . \qquad (28)$$

Similarly, for interstitials

$$P_{tot}^{ie} = P_C^{ie} + P_d^{ie} + P_{GB}^{ie} + P_R^{iv} , \qquad (29)$$

where P_R^{iv} is the thermal Frenkel pair production term ($\alpha C_{vu} C_{iu}$).

3.3. Rate equations

The assumption that microstructural changes preserve the fuel chemical composition (i.e. UO$_{2\pm x}$) reduces the complexity of the problem to only studying uranium metal point defect diffusion. The

mobilities of metal point defects is lower than those for oxygen (table 1), and hence they are rate controlling. The time rate of change of uranium metal vacancy and interstitial concentrations are then given by

$$\frac{dC_v}{dt} = P_{tot}^{ve} + P - P_{sv} - P_r , \qquad (30)$$

and

$$\frac{dC_i}{dt} = P_{tot}^{ie} + P - P_{si} - P_r . \qquad (31)$$

P is the fractional rate of point defect production, and is expressed as

$$P = Y_{iv} \dot{F}_f \Omega \text{ at/at} \cdot \text{s} . \qquad (32)$$

Y_{iv} is the number of Frenkel pairs per fission event and $\dot{F}_f$ is the fission rate.

Finally, the cavity radius rate of change is determined by considering the vacancy and interstitial fluxes * received by and emitted from the cavity. Denoting the matrix point defect fluxes by $\phi_{v,i}$, and the point defect fluxes at the surface of the cavity by $\phi_{v,i}^e$, we can write:

$$\phi_v = D_v C_v , \qquad \text{cm}^2/\text{s} \qquad (33)$$

$$\phi_i = D_i C_i , \qquad \text{cm}^2/\text{s} \qquad (34)$$

$$\phi_v^e = D_v C_{vu} \exp\{F_m \Omega/kT\}, \quad \text{cm}^2/\text{s} \qquad (35)$$

$$\phi_i^e = D_i C_{iu} \exp\{-F_m \Omega/kT\}. \quad \text{cm}^2/\text{s} \qquad (36)$$

Now the rate equation for the cavity radius is given by

$$\frac{dR_c}{dt} = \frac{1}{R_c}\{\phi_v - \phi_i - \phi_v^e + \phi_i^e\}, \qquad (37)$$

where R_c is the cavity radius in cm The last equation is based on a diffusion limited model for cavity growth and shrinkage kinetics [20].

When irradiation production of point defects is dominant, the concentrations, C_v and C_i, can be many orders of magnitude greater than their thermal equi-

librium values. The defect emission fluxes of the cavity are negligible in these cases and the growth is determined by the bulk fluxed, ϕ_v and ϕ_i. However, at high temperatures the thermal emission of point defects from the microstructural sinks will dominate. The concentrations of vacancies and interstitials then approach their thermal equilibrium and the radius of the cavity tends to the equilibrium value that sets the mechanical driving force, F_m, equal to zero.

3.4. Computational aspects

The simple model presented above allows a systematic study of the effects of material and irradiation variables on bubble growth. In order to perform such studies, a computer code was developed to integrate the rate eqs. (30), (31) and (37) which are assembled in vector notation as:

$$\dot{Y} = f(Y, t) \qquad (38)$$

where t is time. In our particular application of the rate theory, the solution vector has the following components

$$Y(1) = C_v, \quad Y(2) = C_i, \quad Y(3) = R_c . \qquad (39)$$

Each component responds to environmental variations according to its own time scale which is dependent on both temperature and microstructure. Care is required in choosing an integration scheme for systems with widely varying time constants since most methods are stable for time steps on the order of the smallest time scale while interest is often focused on the longest lived phenomena.

Our computer model contains the Gear package which is ideally suited for solving such stiff systems of equations [14]. The main feature of the Gear package is its ability to take time steps on the order of the instantaneous time scale of the system. Hence, short time steps are required only during the life of the short lived phenomena. After their decay, large time steps result in significant savings in computational expense.

4. Reactor start-up results

When uranium oxide fuels are used in power reactors, they experience a time dependent temperature

---

* The term "flux" is used merely to describe flow in and out of the cavity. However, for dimensional consistency with the literature, it can be shown that $\phi \simeq \frac{1}{4}a^4 \times$ atom flux.

dictated by the reactor power history [18]. In this section, we will assume that the temperature is constant during reactor operation. Only the fission rate is a step function of time to simulate reactor start-up conditions. After a period from start-up point defects tend to a quasi-steady state that simultaneously sets dC_v/dt and dC_i/dt equal to zero. Our discussion focuses on the dynamic behavior of the system during and after the establishment of quasi-steady state. The time required to reach quasi-steady state is on the order of the inverse time constant at the irradiation temperature. Material parameters of tables 1 and 2 were adopted throughout the calculations to investigate the effects of fuel temperature and stoichiometry on bubble behavior.

Cavity radius and point defect flux histories for 100 gas atom cavities in stoichiometric uranium oxide at a temperature of 1800 K are shown in fig. 4. The mean interstitial lifetime, $\tau_i = \lambda_i^{-1}$, is on the order of

10^{-9} s at this temperature. Therefore, interstitials quickly achieve a quasi-steady state with the microstructure. However, the less mobile vacancies rise more slowly to their quasi-steady state concentrations ($\tau_v \approx 0.28$ s).

The system would be in a true steady state were it not for the slight preference of dislocations for interstitials ($Z_i/Z_v = 1.02$) which results in a vacancy flux slightly larger than the interstitial flux, $\phi_v/\phi_i = 1.001$. This flux mismatch causes a slow growth of the cavities as shown in fig. 4. As the cavity continues to grow, it becomes underpressurized($2\gamma/R_c > P_g$) and vacancy thermal emission becomes important. At about 2×10^6 s, a steady state is reached when the vacancy and interstitial emission fluxes balance the bias flux ($\phi_v^e - \phi_i^e \simeq \phi_v - \phi_i$). The flow of defects to cavities accounts for $\sim 70\%$ of point defect loss rates, while their mutual recombination provides the rest.

At low temperatures, the relaxation times become

Table 2
Parameter values used in the calculations

Parameter	Notation	Value	Units
Uranium vacancy diffusion coefficient pre-exponential [a]	D_v^o	1.0×10^{-3} [15]	cm^2/s
Uranium interstitial diffusion coefficient pre-exponential [a]	D_i^o	7.12×10^3 [15]	cm^2/s
Ratio of recombination coefficient to interstitial diffusion coefficient [b]	$g = \alpha/D_i$	1.0×10^{16} [16]	cm^{-2}
Dislocation density	ρ_d	1.0×10^8 [2]	cm^{-2}
Vacancy dislocation bias factor	Z_v	1.0	
Interstitial dislocation bias factor	Z_i	1.02	
Bubble concentration	N_C	1.0×10^{16}	cm^{-3}
Van der Waals constant	a	51.0	cm^3/mol
Atomic volume	Ω	4.09×10^{-23}	cm^3
Bubble surface energy	γ	626.0	$ergs/cm^2$
Grain size	d_g	1.0×10^{-3}	cm
Fission rate	$\dot{F}_f$	1.0×10^{13}	cm^{-3}
Fission yield	Y_{iv}	1.0×10^4 [16]	

[a] The pre-exponentials for uranium vacancy and interstitial diffusion were obtained from ref. [15] by using the concentrations at 1600 °C. For O/M = 2.05 a vacancy mechanism is assumed, while for O/M = 1.95 an interstitial mechanism is considered for uranium self diffusion.
[b] Assuming that only uranium interstitials are mobile, the recombination coefficient, α, is defined by α/D_i = constant.
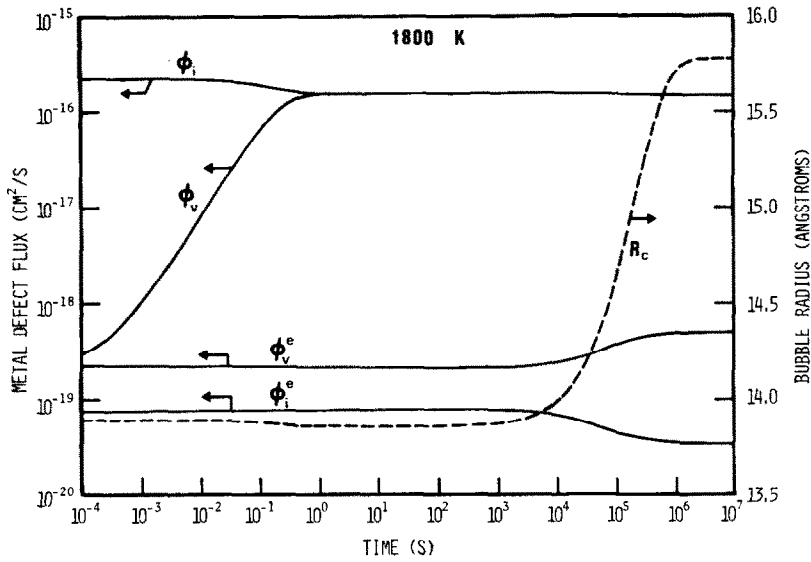
Fig. 4. Flux and radius history for O/M = 2.00 and 100 atoms/bubble at 1800 K.

extremely long. The results for stoichiometric fuels at 1000 K are shown in fig. 5 with $\tau_i \simeq 3 \times 10^{-5}$ s and $\tau_v = 7 \times 10^4$ s. The interstitial flux causes the cavities to shrink until the gas density approaches the Van der Waals limit for xenon, and the cavity can no longer shrink. The cavity radius remains constant until the vacancy flux can reach its quasi-steady state at about 3×10^6 s. Due to the slightly larger vacancy flux, the cavity tends to slowly grow after quansi-steady state conditions have been achieved.

The analysis presented here illustrates the great variations in the magnitudes of the system time scales. Steady state is not immediately satisfied, as assumed in most fuel element models, and a long period of time is needed before such conditions are reached. However, at temperatures greater than ~ 2200 K, thermal point defects are dominant and bubble equilibrium is achieved almost immediately. Bulk and emission point defect fluxes balance each other at the bubble surface. As a result bubbles remain in equilibrium with the matrix, and bubble equilibrium assumptions are justified.
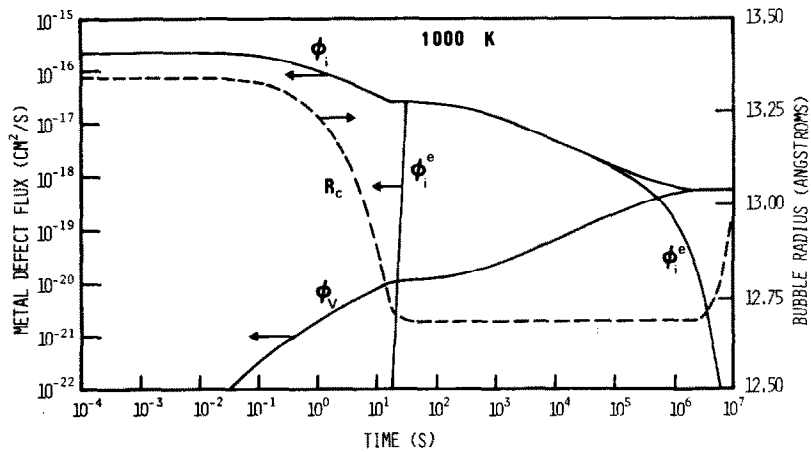

Fig. 5. Flux and radius history for O/M = 2.00 and 100 atoms/bubble at 1000 K.

The response of non-stoichiometric uranium oxide
fuels to irradiation has been investigated at different
fuel temperatures. Point defect thermal equilibrium
concentrations have been found to influence total
point defect concentrations, as well as bubble kinetics.
In fact, the existence of a large thermal interstitial
concentration for hypostoichiometric fuels is respon-
sible for stopping bubble shrinkage faster than the
corresponding stoichiometric case, merely because of
the large emission flux of interstitials from the bubble
surface. On the other hand, hyperstoichiometric Ura-
nium Oxides have abundant thermal equilibrium
vacancies. This tends to maintain the equilibrium
bubble radius unaltered, after the initial shrinkage
transient. For example steady state for $UO_{2.05}$, in
which $\phi_v - \phi_i - \phi_v^e = 0$, is reached at about 3×10^6 s
for the low temperature of only 1000 K. While the
studies presented above do not include gas production
or bubble re-solution during irradiation, they indicate
that steady state fission gas behavior models must
consider point defect dynamic effects. In the next
section we present an investigation of the important
variables affecting uranium oxide response to temper-
ature transients.

5. Thermal transient results

Understanding of bubble response to thermal tran-
sients is of crucial interest to reactor safety studies.
The following investigations simulate bubble behavior
in a temperature ramp from 1000 K to near the melting
point at 3000 K. However, one has to realize that our
formulation does not include the physics of melting.
In all cases the initial cavity radius is the thermal equi-
librium radius and point defects start at their quasi-
steady state concentrations.

5.1. Stoichiometry

Before establishing the efects of different oxygen
to metal ratios on bubble radial changes in a transient,
we will consider the detailed study of a reference case
for which O/M = 2.00, n_g = 1000 at/bubble, ramp
rate = 1000 K/s.

Fig. 6 shows the variation of cavity radius as a func-
tion of time for different oxygen to metal ratios. The
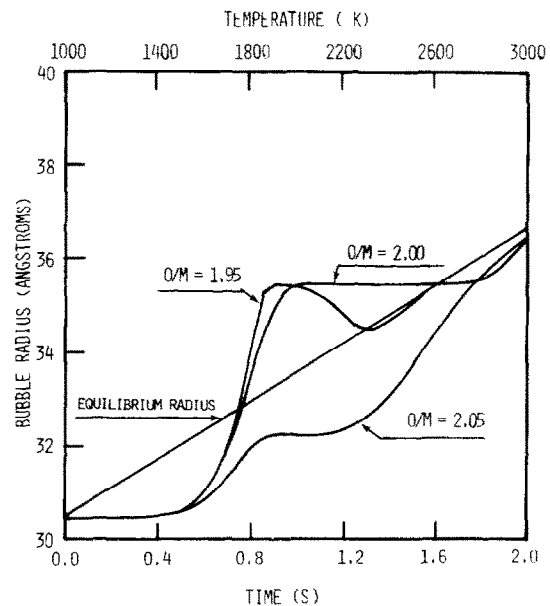equilibrium cavity radius is also plotted on the same

Fig. 6. Bubble radius history for different O/M ratios. Curves
are for 1000 atoms/bubble and 10^3 K/s ramp.

figure, and it is interesting to notice the considerable
deviations of the cavity radius from its equilibrium
value.

At the start of the temperature transient, fission
production of point defects results in steady state con-
centrations many orders of magnitude larger than
their thermal equilibrium values. In fig. 7 the dynamic
and thermal equilibrium point defect concentrations
are shown, while the corresponding defect fluxes are
plotted in fig. 8.

As the temperature increases vacancy mobilities is
enhanced, resulting in a higher vacancy flux. However,
the vacancy concentration does not significantly
change until ~0.75 s when the vacancies become suf-
ficiently mobile to reach the bubbles. Nevertheless,
interstitial concentration goes down because it main-
tains a quasi-steady state between fission production
of point defects and mutual recombination ($P \simeq
\alpha C_i C_v$). On the other hand, the interstitial flux remains
constant as D_i increases, since α is proportional to D_i.
It is important to note that recombination represents
a significant loss mechanism for interstitials but not
for vacancies due to their high concentration.

Cavity growth becomes noticeable when the
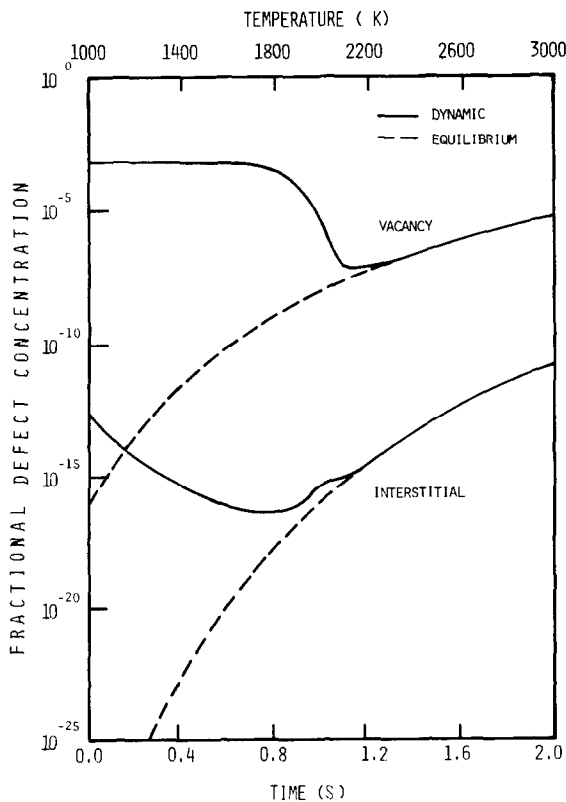vacancy flux becomes appreciable ($> 10^{-14}$ cm^2/s).

Fig. 7. Metal defect history for O/M = 2.00, 1000 atoms/ bubble and a 10^3 K/s ramp.

Fig. 8. Metal flux history for O/M = 2.00, 1000 atoms/ bubble and a 10^3 K/s ramp.

The excess vacancies continue to be absorbed by the cavities until the vacancies reach a quasi-steady state concentration at 1.15 s. As soon as the point defect fluxes drop to insignificant levels, the cavity radius levels off to a plateau that is determined by the initial excess vacancy concentration. After this time, the interstitial fluxes are dominant. The cavities start to grow in response to the increasing temperature at about 1.7 s and 2700 K, when the net interstitial loss from the cavity surface becomes appreciable. At the end of the transient, the bubble tends to its equilibrium size.

The initial system behavior for the hypostoichiometric case, O/M = 1.95, is the same as that for the stoichiometric case because fission production of point defects dominates. However, the interstitial fluxes are much larger as shown in fig. 9 and the cavity reaches the plateau sooner. The net flow of interstitials quickly becomes appreciable and the cavity shrinks to its equilibrium radius. It is interesting to note that uranium self diffusion in $UO_{1.95}$ and above
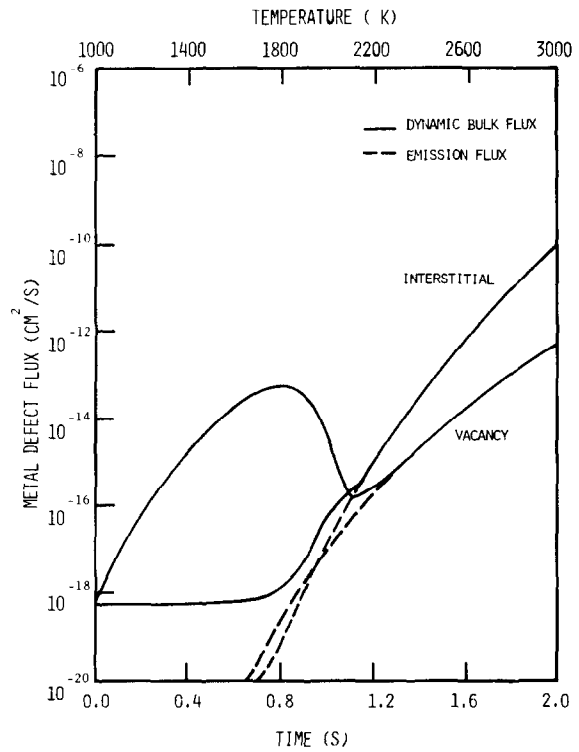
2000 K in UO_2 is based upon an interstitial mechanism.

The thermal equilibrium concentration of vacancies is very high in the hyperstoichiometric case with O/M = 2.05. Cavity response to the temperature ramp is determined by the vacancies which start at only 3.5 times their thermal equilibrium concentration. After the excess vacancies are dumped into the cavities the radius remains constant until the difference between the bulk and emission fluxes of vacancies becomes large enough for the cavity to grow in response to the increasing temperature.

5.2. Ramp rate

Changing the ramp rate does not change the basic features of the results but it does change the temperature at which they occur. Fig. 10 shows the radius history for various stoichiometries when the ramp rate is increased to 10 000 K/s. The excess vacancies and interstitials still flow to the cavities and the cavity
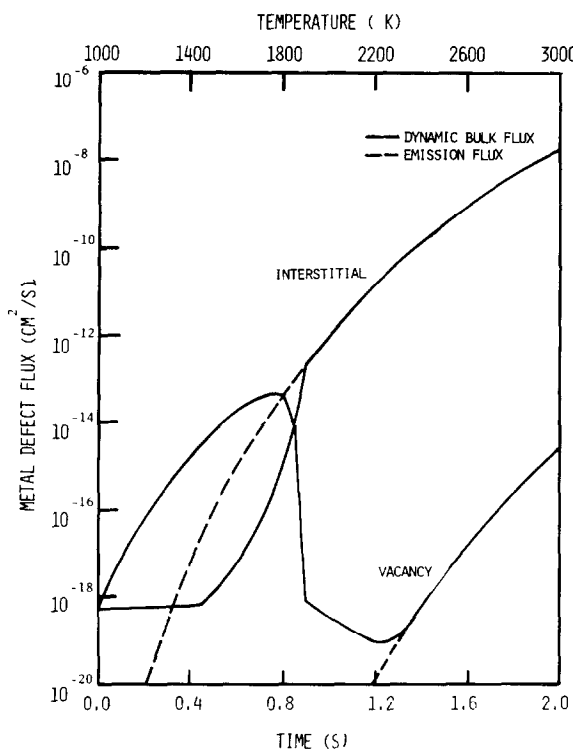
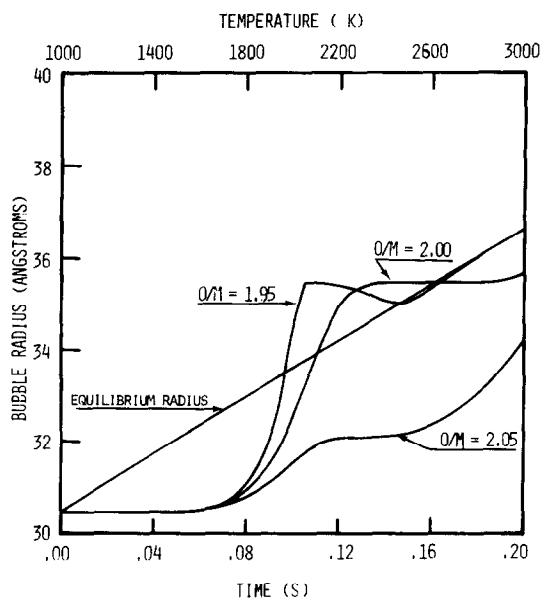Fig. 9. Metal flux history for O/M = 1.95, 1000 atoms/bubble and a 10^3 K/s ramp.

radius plateau for each case is the same as for the 1000 K/s ramp. However, the plateau occurs at a higher temperature since the time scale has been reduced by a factor of ten. It should be noted that for the stoichiometric and hyperstoichiometric cases the cavities are farther from equilibrium at the end of the faster ramp.

5.3. Gas content

Gas content determines the initial size of the cavities and therefore the initial sink strengths for the point defects. The radial changes as functions of time for 1000 K/s ramp, 100 atom bubbles and various stoichiometries are shown in fig. 11. Smaller cavities respond more rapidly to point defect fluxes because they contain fewer vacancies. The deviations from equilibrium are much more extreme than for the 1000 at/bubble simulations, but equilibrium is attained for all stoichiometries by the end of the transient, while it was not for the stoichiometric and hyperstoichiometric 1000 atom bubble cases.
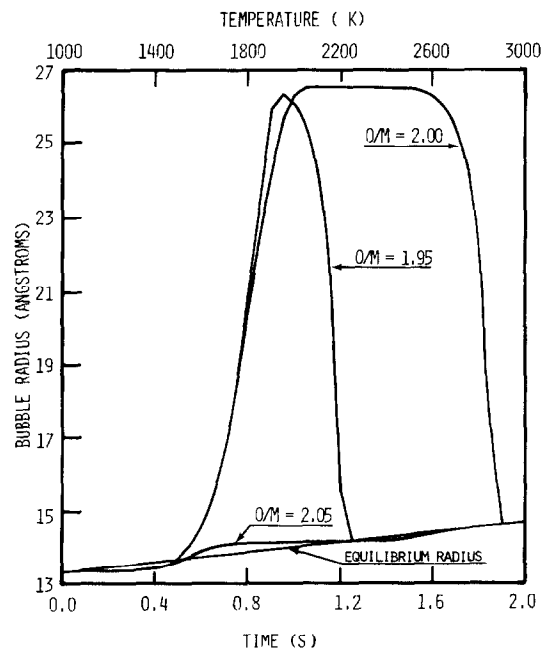

Fig. 10. Bubble radius history for different O/M ratios. Curves are for 1000 atoms/bubble and a 10^4 K/s ramp.

Fig. 11. Bubble radius history for different O/M ratios. Curves are for 100 atoms/bubble and a 10^3 K/s ramp.

5.4. Point defect fission yield and recombination constant

As discussed above, the system response to a thermal transient is first for the excess point defects to flow to the cavity which then adjusts toward equilibrium when the thermal production of point defects becomes dominant. The excess point defects arise from the fission production of Frenkel pairs. In stoichiometric oxide, the main loss of point defects below 1200 K is by mutual recombination, and the quasi-steady state concentrations of vacancies and interstitials are approximately determined by the equations

$$\phi_i \simeq \phi_v , \qquad (40)$$

$$P \simeq \alpha C_i C_v . \qquad (41)$$

Therefore, initially

$$C_v^o = \left(\frac{Y_{iv}}{\alpha/D_i}\right)^{1/2} \left(\frac{\dot{F}\Omega}{D_v}\right)^{1/2} , \qquad (42)$$

$$C_i^o = \left(\frac{Y_{iv}}{\alpha/D_i}\right)^{1/2} \left(\frac{\dot{F}\Omega D_v}{D_i^2}\right)^{1/2} = \frac{D_v}{D_i}C_v . \qquad (43)$$

It can be seen that the ratio of the point defect fission yield, Y_{iv}, to the recombination constant, α/D_i, determines the initial excess point defect concentrations. The 1000 K/s ramp response for 1000 atom cavities and several combinations of Y_{iv} and α/D_i are plotted in fig. 12. It is apparent that the cavity behavior is primarily determined by the initial concentration of point defects which determines the plateau, and the temperature at which the thermal production of point defects becomes dominant. The case with Y_{iv} equal to zero is equivalent to heating without irradiation and point defects start at their thermal equilibrium concentrations.

5.5. Bubble size

In this last section we investigate the effect of initial bubble size on the response of an average bubble to transients. The gas content is considered to be fixed at 10^{19} at/cm^3, while the bubble size is allowed to change. The response of both equilibrium and nonequilibrium bubbles of stoichiometric UO$_2$ to a 1000 K/s transient is shown in fig. 13 for different bubble sizes. The density decreases, as the average
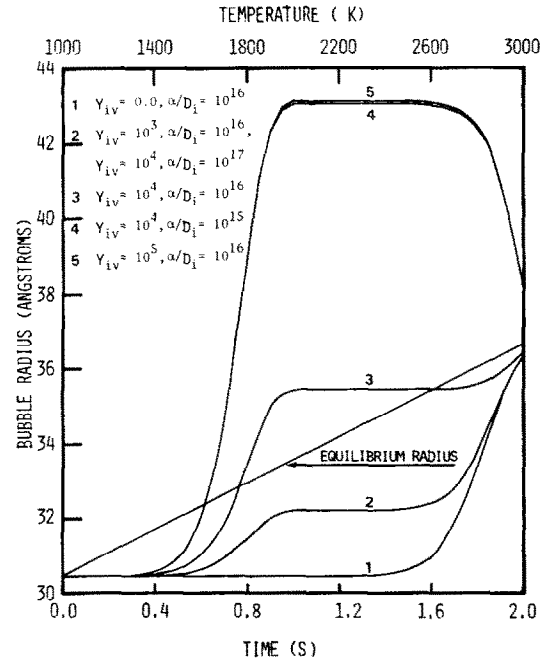

Fig. 12. Radius history for various point defect yields and recombination constants. Curves are for 1000 atom/bubbles O/M = 2.00 and a 10^3 K/s ramp.

bubble radius increases, rendering irradiation induced point defects less effective on the bubble behavior. It is observed that small bubbles (10^3 atoms) become underpressurized for a part of the transient, while large bubbles are overpressurized for the entire transient. For the specific case of 10^5 at/bubble, the bubble internal pressure will exceed the elastic limit of the UO$_2$ matrix ($\sim 5 \times 10^4$ kN/m^2 at 1900 K [19]) after about 0.9 s from the start of the transient. This may lead to localized plastic deformation in the vicinity of the bubble.

The strong effect of bubble size on bubble growth characteristics indicates that the initial bubble distribution may be an important factor in the response of the fuel to a thermal transient. The disposition of intragranular fission gas at the start of an actual reactor transient depends upon the irradiation history. Most of the gas exists as single gas atoms in the fuel matrix with the rest contained in a distribution of various size gas bubbles [21]. The low diffusivity of the bubbles and the short duration of some hypothetical transients allows for very little coalescence [9]. The fission gas response then is limited to the growth
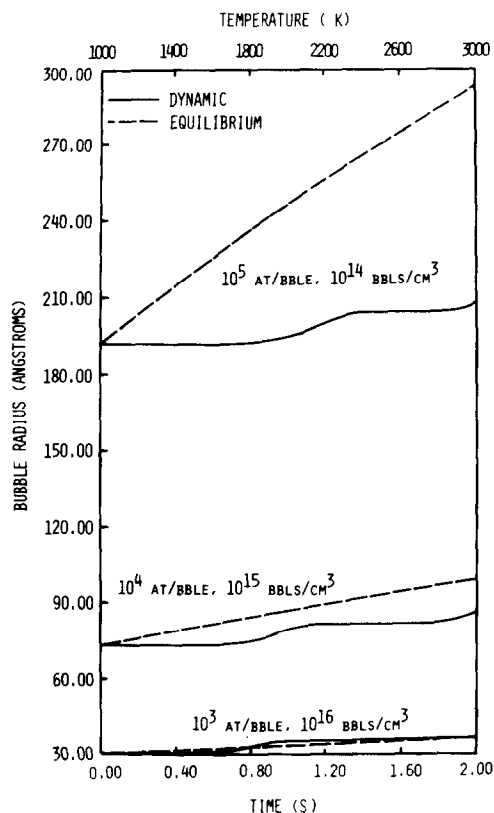
Fig. 13. Radius history for various bubble sizes. Curves are for $O/M = 2.00$ and a 10^3 K/s ramp with a total gas content of 10^{19} atoms/cm^3.

of the existing bubbles due to the increase in temperature and point defect migration. A comprehensive fission gas model, including coalescence and re-solution, is being used to investigate the dynamic behavior of intragranular fission gas [22].

6. Summary and conclusions

During the start-up and transient operation of fast breeder reactors, point defects migrate to existing bubbles with widely varying time scales. The absorption of both vacancies and interstitials and their subsequent emission cause bubbles to experience non-equilibrium radial changes.

Simple thermodynamics has been used to calculate point defect thermal equilibrium concentrations in $UO_{2\pm x}$. Results of the calculations indicate that the interstitial mechanism is dominant for uranium self-diffusion in hypostoichiometric oxides at all temperatures, and in stoichiometric oxides only above 2000 K. This proved to have a considerable effect on bubble kinetics.

Temperature dependent time constants for point defect migration depend on the complex nature of the sink structure as a function of time. At all temperatures, and for start-up conditions, interstitials migrate much faster than vacancies leading to an initial bubble compression stage. The bubble then expands when vacancies reach its surface. However, only at elevated temperatures ($\gtrsim$ 2000 K) does the bubble shrink back to its equilibrium radius, due to the effect of the high vacancy emission rate from its surface. On the other hand, vacancies migrate very slowly at low temperatures leading to a long start-up transient ($\sim 10^6$ s for UO_2 at 1000 K), as the vacancies reach a quasi-steady state with the microstructure.

Thermal ramp behavior of the system has been found to primarily depend on point defect initial concentrations, and on their migration properties. The overall results indicate that the excess point defects find their way quickly to cavities increasing their radius by as much as $\sim$30% above equilibrium (fig. 12). The increasing cavity pressure, as the temperature increases, leads to an asymptotic approach to the equilibrium size. If the temperature increases quickly during the ramp ($\gtrsim 10^3$ K/s), equilibrium bubble size is not attained, even for temperatures as high as the fuel melting point. Fuel stoichiometry has been found to play an important role in determining the rate at which bubbles approach equilibrium, with hypostoichiometric fuels being the fastest.

In conclusion, it is suggested that fuel stoichiometry and the dynamic behavior of point defects should be considered in fuel modeling calculations during start-up and transients, if accurate predictions are expected.

References

[1] D. Stahl and T.J. Patrician, ANL Rept. 8069 (1974).

[2] H.R. Warner and F.H. Nichols, Nucl. Appl. Technol. 9 (1970) 148.

[3] R.B. Poeppel, Fast Reactor Fuel Element Technology, ed. R. Farmakes (ANS, Hinsdale, 1971) p. 311.

[4] C.C. Dollins and F.A. Nichols, J. Nucl. Mat. 66 (1977) 143.

[5] M.R. Haynes and M.H. Wood, J. Nucl. Mat. 67 (1977) 155.

[6] T.D. Gulden and J.L. Kaae, J. Nucl. Mat. 32 (1969) 168.

[7] M.R. Haynes, private communications.

[8] J.W. Harrison, J. Nucl. Mat. 23 (1967) 139.

[9] J.M. Griesmeyer and D. Okrent, ANS Trans. 27 (1977) 322.

[10] Hj. Matzke, Plutonium and Other Actinides, eds. H. Blank and R. Linder (North-Holland, Amsterdam, 1976) p. 801.

[11] G.E. Murch and R.J. Thorn, J. Nucl. Mat. 71 (1978) 219.

[12] N.M. Ghoniem and G.L. Kulcinski, J. Nucl. Mat. 69 & 70 (1978) 816.

[13] L.B. Loeb, The Kinetic Theory of Gases (Dover, New York, 1961) p. 140.

[14] A.C. Hindmasch, LLL Report UCID0-30001, Rev. 3 (1974).

[15] Hj. Matzke, J. de Phys. Suppl. nr. 11–12, 34 (1973) C9-317.

[16] D.R. Olander, Fundamental Aspects of Nuclear Reactor Fuel Elements, Technical Information Center, ERDA, TID-26711-PI (1976).

[17] P.S. Maiya, J. Nucl. Mat. 40 (1971) 57.

[18] M.J.F. Notley and J.R. MacEwan, Nucl. Appl. 2 (1966) 117.

[19] R.F. Canon, J.T.A. Roberts and R.J. Beals, J. Am. Ceram. Soc. 54 (1971) 105.

[20] N.M. Ghoniem, Ph.D. Thesis, University of Wisconsin (1977).

[21] C. Baker, J. Nucl. Mat. 67 (1977) 283.

[22] J.M. Griesmeyer, Ph.D. Thesis, University of California (1979).